

# CO<sub>2</sub> Capture by Using a Membrane-Absorption Hybrid Process in the Nature Gas Combined Cycle Power Plants

Wenfeng Dong\*, Mengxiang Fang, Tao Wang, Fei Liu, Ningtong Yi

*State Key Laboratory of Clean Energy Utilization, Zhejiang University,  
Hangzhou 310027, People's Republic of China*

## Abstract

The main research objective of this paper was to optimize the design parameters of the hybrid membrane - absorption CO<sub>2</sub> capture process in Natural Gas-steam Cycle (NGCC) power plants. To predict the CO<sub>2</sub> concentration in permeate gas and required membrane area, a mass transfer calculation model of CO<sub>2</sub>/N<sub>2</sub>/H<sub>2</sub>O separation membrane was established in Aspen plus. Effect of CO<sub>2</sub> recovery rate of membrane unit, operating pressure proportion of feed gas pressure over permeate gas pressure and flue gas flow ratio on membrane area, compressor power and solution regeneration duty were studied based on membrane calculation model. The optimal parameter of feed/permeate side pressure ratio and flow ratio are 10:1 and 50% respectively. The solution regeneration duty of hybrid process reduced at over 20.7% than traditional chemical absorption process.

**Keywords:** Membrane-absorption process; Mass transfer model; Natural Gas-Steam Combined Cycle power plants; CO<sub>2</sub> capture; Monoethanolamine.

## INTRODUCTION

Carbon capture, utilization and storage (CCUS) technologies was mainly applied in the coal-fired field due to the carbon emission of coal-fired power plant was over twice for NGCC (Natural Gas Steam Cycle) power plants (Yu et al, 2012). As a relatively clean energy, natural gas is widely used in various industrial fields. CO<sub>2</sub> reductions from NGCC (Natural Gas Steam Cycle) power plants had a better application prospect in the long run. For an NGCC power plant with capacity of approximately 390 ~ 1600 MW<sub>e</sub>, the carbon emissions from the flue gas was approximately 190~600 kg MW<sup>-1</sup> (Martin-Gamboa *et al.*, 2018). Considering the considerable

---

\* Corresponding author. Tel: 1-599-016-4885;

E-mail address: wfdong@zju.edu.cn

30 carbon emission of the NGCC power plant, CO<sub>2</sub> capture in the NGCC power plants will become  
31 an significance technical storage from a longer term perspective. While CO<sub>2</sub> concentration of the  
32 flue gas in NGCC power plant was about 4 vol.% due to high excess air ratio.

33 For the coal-fired power plant, the optimal regeneration duty of 30 wt.% Monoethanolamine  
34 (MEA) solution was about 3.6 ~ 4.5 GJ t<sup>-1</sup> CO<sub>2</sub> with 80% ~ 90% of the CO<sub>2</sub> capture rate (Artanto  
35 *et al.*, 2012; Mangalapally *et al.*, 2012; von Harbou *et al.*, 2012; Rabensteiner *et al.*, 2014; Oh *et*  
36 *al.*, 2016). Therefore, high equipment disposable investment, solution regeneration duty and  
37 operating cost of CO<sub>2</sub> capture became the major obstacles of preventing large-scale adoption.  
38 Efforts of reducing carbon capture cost had been made on three major aspects: optimizing  
39 operational parameters, process modifications (Le *et al.*, 2011; Ahn *et al.*, 2013; Yang *et al.*, 2020)  
40 and developing better solvents (Yu *et al.*, 2019; Liu *et al.*, 2019; Yu *et al.*, 2020) .

41 However, the power plant with the CO<sub>2</sub> capture process would result in reduction of power  
42 generation efficiency. Especially, CO<sub>2</sub> concentration of the flue gas in NGCC power plant (4  
43 vol.%) was much lower than that in coal-fired power plant (10 ~ 14 vol.%). The driving force  
44 was relatively weak due to lower CO<sub>2</sub> concentration of the lower part of the absorber, which  
45 resulting high solution flow and solution regeneration duty. The testing CO<sub>2</sub> partial pressure of  
46 flue gas was about 55 mbar, and the CO<sub>2</sub> capture rate was over 90%. When the structured  
47 packing 250.Y height over 12 m, the rich CO<sub>2</sub> loading was raised to 0.44 mol. CO<sub>2</sub> mol.<sup>-1</sup> MEA  
48 (Notz *et al.*, 2012; Agbonghae *et al.*, 2014). The optimal solution regeneration duty was about  
49 3.7-4.2 GJ t<sup>-1</sup> CO<sub>2</sub> (Li *et al.*, 2011; Mores *et al.*, 2014; Amann *et al.*, 2009; Luo *et al.*, 2015; Luo  
50 *et al.*, 2016). While the solution regeneration duty had a significant linear correlation with the  
51 effective mass transfer area, which was related to the specific surface area and height of the  
52 structured packing. The measured solution regeneration duty were all over 7.0 GJ t<sup>-1</sup> CO<sub>2</sub> when

53 the CO<sub>2</sub> concentration was less than 5.5%. So the practical solution regeneration duty was higher  
54 than the mentioned values above due to the lower rich CO<sub>2</sub> loading (Akram *et al.*, 2016).

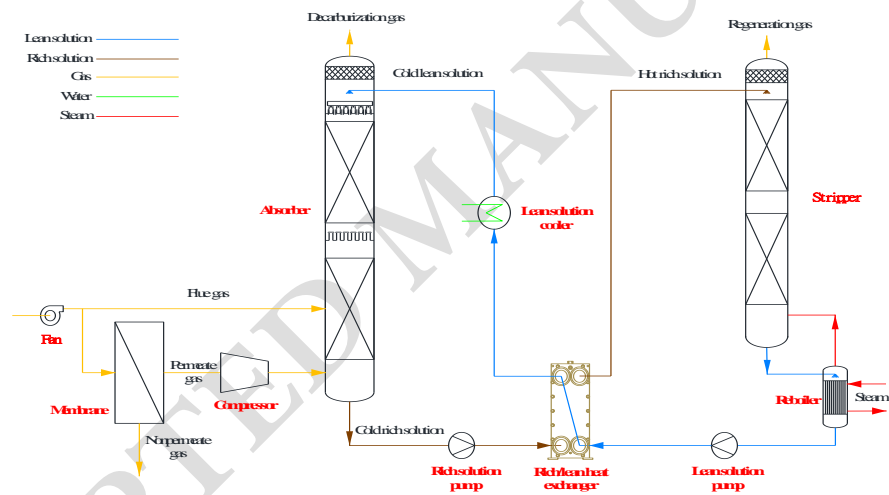
55 To improve the driving force of the lower part of the absorber, Membrane Technology and  
56 Research (MTR) and the University of Texas at Austin previously proposed a hybrid system  
57 which considering amine scrubbing and membrane process (Freeman *et al.*, 2014). Maintaining  
58 the uniform overall CO<sub>2</sub> capture rate, CO<sub>2</sub> concentration of the flue gas could be enriched from  
59 12% to 23% by using CO<sub>2</sub> enrichment membrane, and flue gas flowrate will be reduced to 47%  
60 accordingly. CO<sub>2</sub> concentration increased from 14% to 28%, which increasing the mass transfer  
61 driving force in the absorber (Frimpong *et al.*, 2019). CO<sub>2</sub> concentration in the flue gas was  
62 raised to 12 vol.% with membrane unit in NGCC power plant. The total cost of the hybrid amine /  
63 membrane system was lowest when CO<sub>2</sub> concentration enriched to 12% (Ding *et al.*, 2017). The  
64 flue gas split ratio in the membrane unit was calculated by ChemCAD, and absorber with a direct  
65 contact cooler (DCC) or pump-around, and variable lean loading was optimized in Aspen Plus.  
66 MATLAB software was also used to simulate the three-stage membrane process for CO<sub>2</sub>  
67 separation (Liu *et al.*, 2019). Few literature on mass transfer calculation model in aspen plus  
68 software. Few researchers concerned the simulation of the membrane-absorption hybrid process.  
69 While ChemCAD and MATLAB software were just used for calculating the membrane process.  
70 CO<sub>2</sub> recovery rate and CO<sub>2</sub> concentration of membrane unit will affect the absorption process. So  
71 ChemCAD and MATLAB software had no special advantages in calculating the overall  
72 performance of the hybrid process.

73 In this paper, the effect of CO<sub>2</sub> capture rate, specific surface area of structured packing, lean  
74 CO<sub>2</sub> loading and stripper pressure in the CO<sub>2</sub> capture process with 30 wt.% MEA solution were  
75 studied. The mass transfer model of CO<sub>2</sub>/N<sub>2</sub>/H<sub>2</sub>O separation membrane was established based on  
76 the hybrid membrane/30 wt.% MEA process. Effect of CO<sub>2</sub> recovery rate of the membrane unit,

77 operating pressure proportion of feed gas pressure over permeate gas pressure and flue gas flow  
 78 ratio on membrane area, compressor power and solution regeneration duty were studied based on  
 79 the membrane calculation model.

## 80 METHODS

81 To improve the driving force of gas/liquid reaction in the lower part of the absorber, a portion  
 82 of the flue gas was first pumped into the membrane separation unit. CO<sub>2</sub> concentration of the flue  
 83 gas was enriched to above 20 vol.% in permeate gas, which could increase the rich CO<sub>2</sub> loading.  
 84 This effect just worked in the lower part of the absorber, so the residual flue gas directly pumped  
 85 into the upper part of the absorber, as shown in Fig. 1.



86  
 87 **Fig. 1.** Membrane - absorber hybrid CO<sub>2</sub> capture process in NGCC power plant.

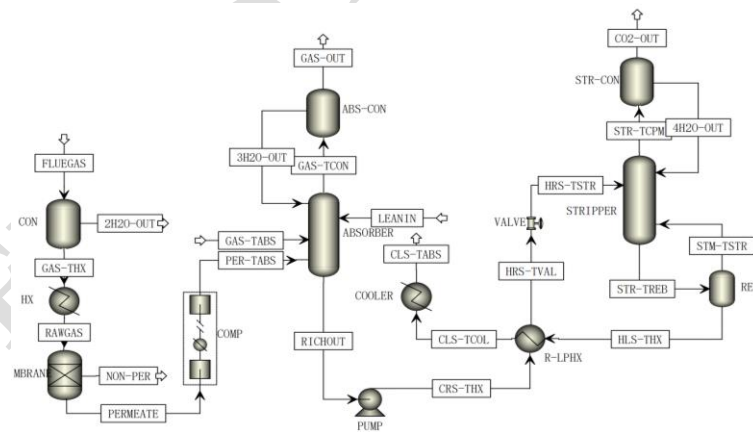
88 The flow of the flue gas was about 21,600 Nm<sup>3</sup> h<sup>-1</sup>, the CO<sub>2</sub> capture scale was 12,000 tons a<sup>-1</sup>,  
 89 and the annual operation time was 7,500 hr a<sup>-1</sup> in the simulation. The CO<sub>2</sub> capture rate ranged  
 90 from 50% to 90%. The specific components, pressure and temperature of the flue gas were shown  
 91 in **Table 1**.

92  
 93 **Table 1.** Base parameter of flue gas in the NGCC power plant

Parameters	Units	Value
------------	-------	-------

Composition		
CO <sub>2</sub>	vol.%	4.20
O <sub>2</sub>	vol.%	5.00
N <sub>2</sub>	vol.%	81.77
H <sub>2</sub> O	vol.%	7.03
Pressure	bar	1.06
Temperature	°C	40

94 Aspen plus software was applied in CO<sub>2</sub> capture process from the flue gas in the power plant  
95 with MEA solution. Rigorous physical and chemical properties were needed for evaluating the  
96 performance of the CO<sub>2</sub> capture process by using 30 wt.% MEA solution. The electrolyte non-  
97 random two-liquid (e-NRTL) method and PC-SAFT equation of state were used to compute  
98 liquid and vapor properties of the CO<sub>2</sub>-MEA-H<sub>2</sub>O system, respectively. The rate-based model of  
99 CO<sub>2</sub>-MEA-H<sub>2</sub>O system had been validated with pilot testing results. Based on the diffusion  
100 model, the hybrid membrane/absorption process of the CO<sub>2</sub> capture in NGCC power plant was  
101 built in Aspen plus, as shown in **Fig. 2**. In order to reduce the compressor power of the hybrid  
102 process, the vacuum compressor was applied instead of compressor.



103  
104 **Fig. 2.** Hybrid membrane-absorption process of CO<sub>2</sub> capture.

105 The composition of actual exhaust gas was complex, which will affect the performance of the  
106 absorption process. In order to simplify the simulation process, the following hypothesis was  
107 proposed: (1) The flue gas temperature was set as 40°C, and the ash and nitrogen sulfur oxides  
108 were ignored; (2) Degradation of solvent and corrosion of equipment were not considered in the

109 simulation; (3) CO<sub>2</sub>, O<sub>2</sub> and N<sub>2</sub> were selected as Henry gas, which conformed to Henry's law; (4)  
 110 All heat and mass transfer equipment and process were set as heat insulation. 30 wt.% MEA  
 111 aqueous solution was selected as absorption solution. The temperature difference of the rich/lean  
 112 solution heat exchanger between cold lean solution and cold rich solution was set as 5°C. **Table.**  
 113 **2** listed the diameter, packing type and model parameters of absorber and stripper. Bravo (1992)  
 114 fitting equation was adopted to determine the effective mass transfer area of the structured  
 115 packing in absorber and stripper.

116 **Table 2.** Settings in the rate-based calculation

Items	Absorber	Stripper
Packing type	Mellapak 250.Y	Mellapak 500.Y
Packing height	30 m	10 m
Column diameter	2.2 m	1.4 m
Flow model	Mixed model	Mixed model
Film resistance	Discrxn for liquid, film for vapor	
Interfacial area method	Bravo, 1992	

117  
 118 The operating principle of the membrane unit was that different gas molecules had disparate  
 119 permeation rates through membrane pores under a certain pressure difference. The permeability  
 120 coefficient of gas in membrane structure was an important parameter, which directly affected the  
 121 membrane area and CO<sub>2</sub> recovery rate. The calculation method of membrane area and CO<sub>2</sub>  
 122 recovery rate were shown in Eqs. (1, 2):

$$A_{mCO_2} = \frac{y_{CO_2P} U_P}{J_{CO_2} (xP - yP_{CO_2})} \quad (1)$$

$$\theta_{CO_2} = \frac{J_{CO_2} (xP - yP_{CO_2}) A_{mCO_2}}{x_{CO_2F} U_F} \quad (2)$$

126 Where,  $A_{mCO_2}$  was the membrane area, m<sup>2</sup>;  $\theta_{CO_2}$  was the CO<sub>2</sub> recovery rate;  $x_{CO_2F}$  and  $y_{CO_2P}$   
 127 were the CO<sub>2</sub> concentration in feed and permeability gas, respectively;  $U_F$  and  $U_P$  were the total

128 flow of feed and permeability gas, respectively,  $\text{kmol h}^{-1}$ ;  $J_{\text{CO}_2}$  was the permeability coefficient,  
 129  $\text{kmol h}^{-1} \text{m}^{-2} \text{kPa}^{-1}$ ; and  $\overline{xP - yP_{\text{CO}_2}}$  was the  $\text{CO}_2$  average differential pressure.

130 Recent years had seen great advances in membrane technology (Mubashir et al. 2018). A  
 131 membrane unit specifically developed by MTR for this application (called Polaris™), with pure-  
 132 gas  $\text{CO}_2$  permeance values =1000 ~ 2000 GPU (50 psig, 23°C) and  $\text{CO}_2/\text{N}_2$  selectivity=50 ~ 60  
 133 (White et al., 2015; Xu et al., 2019). In this paper, plate and frame modules of membrane unit  
 134 with 1500 GPU and 30  $\text{CO}_2/\text{N}_2$  selectivity was applied. As shown in Fig. 3, the  $\text{CO}_2$  recovery rate  
 135 and desired membrane area of  $\text{CO}_2/\text{N}_2/\text{H}_2\text{O}$ , the mass transfer model of separation membrane was  
 136 built in Aspen plus calculator. The selectivity of  $\text{CO}_2/\text{H}_2\text{O}$  was set as 1, so the permeability  
 137 coefficient of  $\text{H}_2\text{O}$  was identical with that of  $\text{CO}_2$ . The  $\text{CO}_2$  concentration had been elevated to  
 138 more than 20 vol.% in the permeate gas.

Design specification $\theta_i = \frac{y_{iF}U_F}{x_{iF}U_F}$												
Recovery	$\theta_{\text{CO}_2F}$	0.2500	-	$\text{CO}_2$	1500	GPU						
	$\theta_{\text{H}_2\text{OF}}$	0.2800	-	$\alpha_{\text{CO}_2/\text{N}_2}$	30	-						
	$\theta_{\text{N}_2F}$	0.0270	-	$\alpha_{\text{CO}_2/\text{H}_2\text{O}}$	1	-						
Variate	Flue gas		Non-permeate gas		Permeate gas		Units		Average partial pressure difference			
Flow	$U_F$	1341.288	$U_R$	1277.0545	$U_p$	52.49475		$\text{kmol/h}$	$\overline{xP - yP_{\text{CO}_2}}$	0.933508	kPa	$\overline{xP - yP_i} = x_iP - y_iP$
Pressure	$P_F$	106	$P_R$	106	$p$	10		$\text{kPa}$	$\overline{xP - yP_{\text{H}_2\text{O}}}$	0.766892	kPa	
Composition	$x_{\text{CO}_2F}$	0.030238	$x_{\text{CO}_2R}$	0.0238191	$y_{\text{CO}_2p}$	0.193151		-	$\overline{xP - yP_{\text{N}_2}}$	93.03168	kPa	
	$x_{\text{H}_2\text{OF}}$	0.022256	$x_{\text{H}_2\text{OR}}$	0.0168305	$y_{\text{H}_2\text{Op}}$	0.159226		-	Plate separation membrane			
	$x_{\text{N}_2F}$	0.938754	$x_{\text{N}_2R}$	0.9593504	$y_{\text{N}_2p}$	0.647622		-	Permeability coefficient	$J_{\text{CO}_2}$	1.80E-03	$\text{kmol}/(\text{h} \cdot \text{m}^2 \cdot \text{kPa})$
	$\theta_i = \frac{y_{iF}U_F}{x_{iF}U_F}$									$J_{\text{H}_2\text{O}}$	1.80E-03	$\text{kmol}/(\text{h} \cdot \text{m}^2 \cdot \text{kPa})$
	$y_{\text{CO}_2p} + y_{\text{H}_2\text{Op}} + y_{\text{N}_2p} = 1$									$J_{\text{N}_2}$	6.00E-05	$\text{kmol}/(\text{h} \cdot \text{m}^2 \cdot \text{kPa})$
	$x_{iF}U_F = x_{iR}U_R + y_{iF}U_p$								$A_{\text{mCO}_2}$	6034.25	$A_m = \frac{y_{iF}U_F}{J_i(xP - yP_i)}$ $\theta_i = \frac{J_i(xP - yP_i)A_m}{x_{iF}U_F}$	
	$x_{\text{CO}_2R} + x_{\text{H}_2\text{OR}} + x_{\text{N}_2R} = 1$								$A_{\text{mH}_2\text{O}}$	6055.14		
								$A_{\text{mN}_2}$	6090.54			

139  
 140 Fig. 3. Mass transfer model of  $\text{CO}_2/\text{N}_2$  separation membrane in Aspen plus calculator

## 141 RESULTS AND DISCUSSION

### 142 Structured packing

143 The structured packing, as the core part of mass and heat transfer in the absorber, which  
 144 determined the gas-solution flow mode and mass transfer coefficient. The structural parameter of  
 145 the structured packing directly affected the absorption performance, such as absorber diameter,

146 pressure drop of the structured packing section, rich CO<sub>2</sub> loading, solution flow and solution  
147 regeneration duty. According to the two-film mass transfer theory, the mass transfer process was  
148 theoretically controlled by Henry constant of gas physical dissolution in the CO<sub>2</sub>-MEA  
149 absorption process. In the solution phase, the effect of gas/liquid reaction was expressed by the  
150 chemical enhancement factor  $E=k_L/k_L^0$ . The total mass transfer coefficient in the absorber with  
151 the reaction between CO<sub>2</sub> and amine solution was as follows:

152

$$153 \quad K_G a_e = a_e \cdot \frac{E k_L}{H e} = a_e \cdot \frac{\sqrt{k_2 [MEA] D_{CO_2,l}}}{H e} \quad (3)$$

154 The gas/liquid reaction of the lower part of the absorber was controlled by the thermodynamic,  
155 while upper part was controlled by the dynamics. As a result, the reaction rate increased first and  
156 then decreased along with the structured packing height. For the NGCC power plant, the CO<sub>2</sub>  
157 partial pressure of the flue gas was low (about 4.0 vol.%), the driving force of the reaction of the  
158 lower part of absorber was weak. In order to achieve 90% of the capture rate from the flue gas in  
159 NGCC power plant, higher specific surface area of the structured packing was needed. **Fig. 4**  
160 showed the effect of packing height on flooding point and rich CO<sub>2</sub> loading. As the height of  
161 structured packing increased, the effective gas/liquid mass transfer area expanded, the gas-liquid  
162 contact time extended, the rich solution CO<sub>2</sub> loading increased, and the solution flow rate  
163 decreased. When the height of structured packing 250.Y ranged from 16 m to 30 m, the rich  
164 solution CO<sub>2</sub> loading increased from 0.294 to 0.396 mol. CO<sub>2</sub> mol.<sup>-1</sup> MEA, and the flooding point  
165 reduced to 60.9% simultaneously.



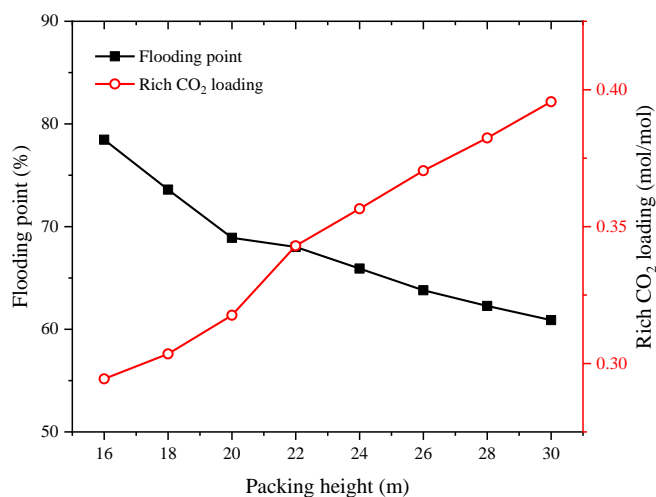
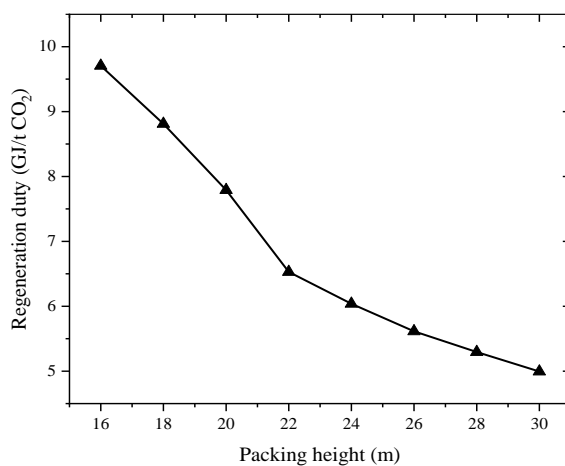


**Fig. 4.** Effect of packing height on rich CO<sub>2</sub> loading and flooding point of absorber

166

167

168 The rich CO<sub>2</sub> loading and solution flow affected the latent heat of the CO<sub>2</sub> product gas which  
 169 out from the stripper and sensible heat of the hot rich/lean solution in the regeneration process,  
 170 which directly affected the regeneration duty. As shown in **Fig. 5**, the regeneration duty  
 171 decreased with the increasing of the structured packing height. The results demonstrated that the  
 172 optimal parameters selected were 90% CO<sub>2</sub> capture rate, 30m 250Y structured packing, 0.26 mol  
 173 CO<sub>2</sub> mol<sup>-1</sup> MEA lean CO<sub>2</sub> loading and 2.0 bar stripper pressure. Under this operating condition,  
 174 the rich CO<sub>2</sub> loading and solvent regeneration duty were 0.396 mol. CO<sub>2</sub> mol.<sup>-1</sup> MEA and 4.99 GJ  
 175 t<sup>-1</sup> CO<sub>2</sub>, respectively. The regeneration duty can reduced to 4.54 GJ t<sup>-1</sup> CO<sub>2</sub> when the total  
 176 packing volume of 25 m IMTP 40 random packing was about 1.27 times of the 30 m 250.Y  
 177 structured packing in the absorber (Luo *et al.*, 2015).



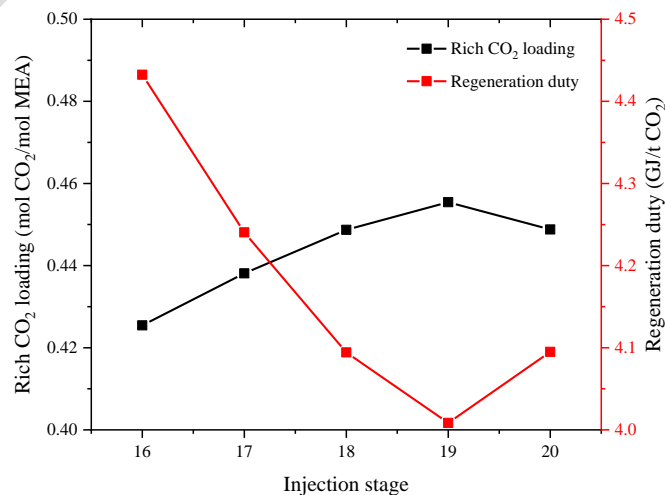
178

179

**Fig. 5.** Effect of packing height on solvent regeneration duty

180 **Flue gas inlet stage**

181 The reaction of the lower part of the absorber was controlled by thermodynamics. In order to  
182 increase the rich CO<sub>2</sub> loading, the permeate gas with higher CO<sub>2</sub> partial pressure should be  
183 pumped into the lower part of the absorber (20 stage, 0m packing location). The flue gas with low  
184 CO<sub>2</sub> partial pressure will affect this absorption process, so the inlet location should be discussed  
185 detailed at first. **Fig. 6** showed the effect of inlet location on the rich CO<sub>2</sub> loading and solution  
186 regeneration duty. With the increasing of the number of flue gas inlet stage, the rich CO<sub>2</sub> loading  
187 increased first and then decreased. Overall, permeate gas with higher CO<sub>2</sub> partial pressure  
188 improved the driving force of the lower part of the absorber. Compared with traditional chemical  
189 absorption process, the higher rich CO<sub>2</sub> loading which resulting the lower solution flow and  
190 solution regeneration duty. When the inlet stage of flue gas with lower CO<sub>2</sub> pressure was over 19  
191 stage (1.5m packing location), the rich CO<sub>2</sub> loading will be reduced, and the regeneration energy  
192 consumption will increase sharply due to the mixture of flue gas with lower CO<sub>2</sub> partial pressure  
193 and permeate gas with higher CO<sub>2</sub> concentration. The optimal inlet stage of the absorber: 18 stage  
194 (1.5 m packing location). The rich CO<sub>2</sub> loading was 0.455 mol. CO<sub>2</sub> mol.<sup>-1</sup> MEA, and the  
195 minimum regeneration energy consumption was 4.01 GJ t<sup>-1</sup> CO<sub>2</sub> under this operating condition.  
196 In this study, 19 stage was selected as the inlet stage of the flue gas with low CO<sub>2</sub> partial pressure.

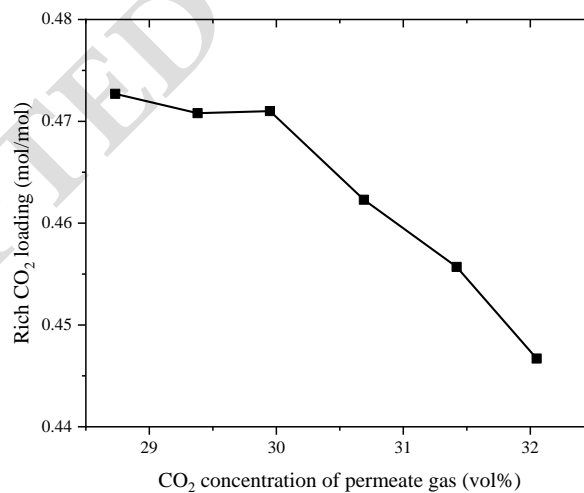


197

198 **Fig. 6.** Effect of flue gas inlet stage on rich CO<sub>2</sub> loading and solvent regeneration duty

199 **CO<sub>2</sub> recovery rate of membrane unit**

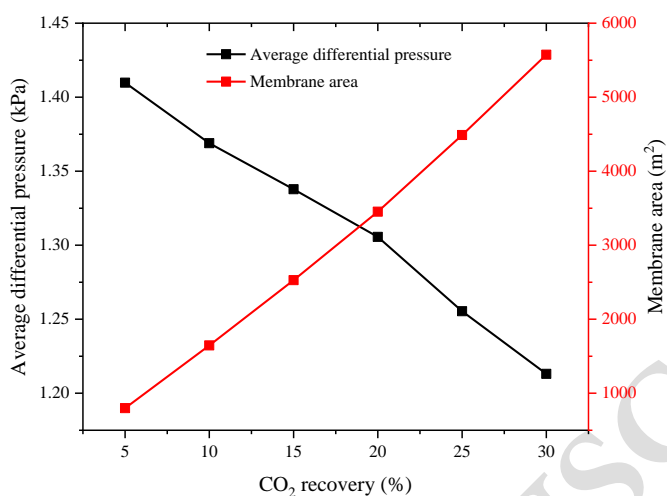
200 The CO<sub>2</sub> recovery rate of the flue gas directly affected the permeated CO<sub>2</sub> concentration and  
201 membrane area, and then affects the rich CO<sub>2</sub> loading, solvent flow and regeneration duty of the  
202 hybrid membrane-absorption process. Therefore, it is necessary to study the effect of CO<sub>2</sub>  
203 recovery on the absorption process. As shown in **Fig. 7**, the permeate gas decreased slightly from  
204 32.3 vol.% to 28.7 vol.% with increasing of flue gas CO<sub>2</sub> recovery rate (5% ~ 30%). The total  
205 cost of the hybrid amine/membrane system is lowest at 12% absorber inlet CO<sub>2</sub>, and the flue gas  
206 split ratio was calculated by ChemCAD (Ding *et al.*, 2017). While the actual CO<sub>2</sub> concentration  
207 of the permeate gas was higher than the value which calculated by ChemCAD. The non-permeate  
208 gas CO<sub>2</sub> concentration had not changed much. The rich CO<sub>2</sub> loading increased with increasing of  
209 CO<sub>2</sub> recovery rate, which still far away from the saturation state. When the CO<sub>2</sub> recovery rate was  
210 over 20%, the rich CO<sub>2</sub> loading had not changed much. The total CO<sub>2</sub> capture capacity improved  
211 with the increasing of CO<sub>2</sub> recovery rate, while the solution flow did not change much.



212 **Fig. 7.** Effect of CO<sub>2</sub> recovery rate on rich CO<sub>2</sub> loading

213 As shown in **Fig. 8**, the average differential pressure of feed/permeate gas and the membrane  
214 area showed an approximate linear with CO<sub>2</sub> recovery rate. The membrane unit operated under  
215

216 atmospheric conditions due to the vacuum compressor. The average differential pressure of the  
217 membrane unit as low as 1.2 ~ 1.42 kPa on this account.



218  
219 **Fig. 8.** Average differential pressure and membrane area

220 For hybrid membrane-absorption process, the compressor power should be taken into account.  
221 The compressor power was linearly relative to the CO<sub>2</sub> recovery rate. The total regeneration duty  
222 included compressor power and solution regeneration duty. The total regeneration duty decreased  
223 first and then increased with the increasing of flue gas CO<sub>2</sub> recovery rate. As shown in **Fig. 9**, the  
224 total regeneration duty ranged from 3.81 ~ 4.12 GJ t<sup>-1</sup> CO<sub>2</sub> when the CO<sub>2</sub> recovery rate ranged  
225 from 5% to 30%. The CO<sub>2</sub> capture scale increased with the increasing of CO<sub>2</sub> recovery of the flue  
226 gas. Considering the membrane area (membrane unit investment) and solvent flow, the optimal  
227 CO<sub>2</sub> recovery rate was selected as 20%.

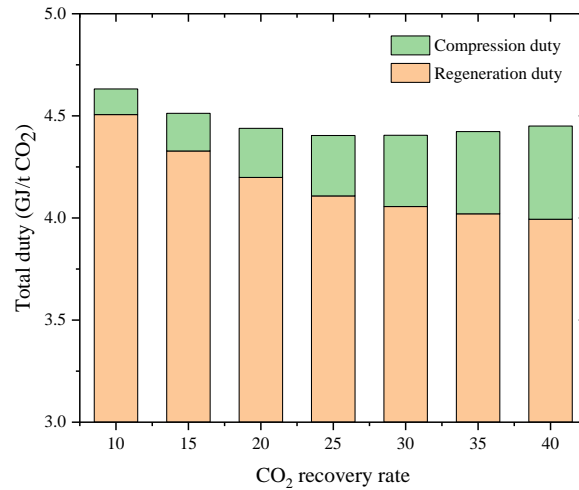


Fig. 9. Effect of CO<sub>2</sub> recovery rate on total duty

228

229

230

231

232

233

234

235

The permeate gas with high CO<sub>2</sub> concentration was pumped into the absorber on 20 stage, and the flue gas with low CO<sub>2</sub> concentration inlet position was set as 19 stage. In such operating condition, these two gases will be inevitably mixed at the position on 18 stage. From Fig. 10, it can be seen that the concentration of flue gas CO<sub>2</sub> changes sharply on 18 ~ 20 stages in the absorber. The CO<sub>2</sub> concentration dropped to about 4.0 vol.% on 19 stage, so it was considered that the two gases were completely mixed at this position.

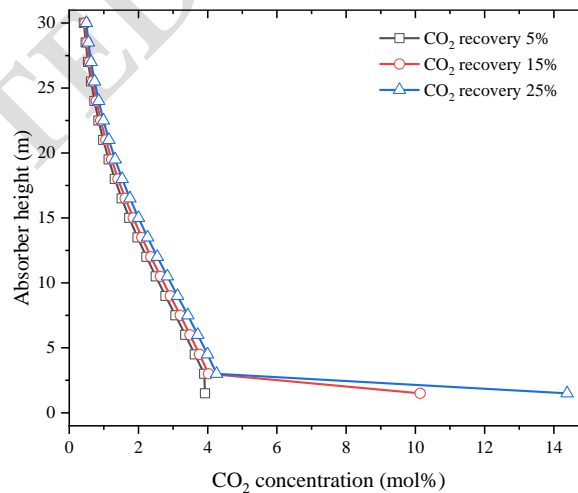


Fig. 10. CO<sub>2</sub> concentration profile of absorber column

236

237

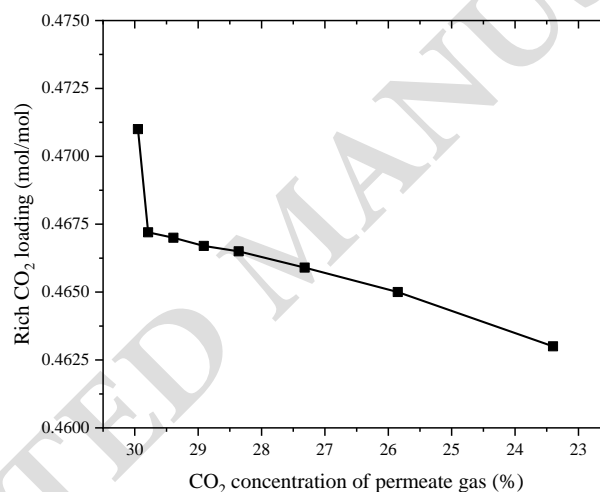
### 238 *Flue gas flow of membrane unit*

239

240

In order to reduce the compressor power, vacuum compressor was applied in the hybrid process. To improve the CO<sub>2</sub> capture rate of the hybrid membrane - absorption process, the flue

241 gas flow of membrane unit should be optimized. At first, the flow of flue gas in membrane unit  
242 was equal to the flow in absorber column. **Fig. 11** showed CO<sub>2</sub> concentration of permeate gas and  
243 rich CO<sub>2</sub> loading under different flue gas flow (100% ~ 30%). Under this condition, CO<sub>2</sub>  
244 concentration reduced from 29.95% to 23.40%. The permeate gas with higher CO<sub>2</sub> partial  
245 pressure will improve the driving force at the bottom of absorber, so the lower CO<sub>2</sub> partial  
246 pressure will result in lower rich CO<sub>2</sub> loading. CO<sub>2</sub> concentration of permeate gas had less effect  
247 on the rich CO<sub>2</sub> loading and solution regeneration duty. The increasing of permeate gas flow  
248 which resulting in higher compressor power due to the decreasing CO<sub>2</sub> concentration of permeate  
249 gas. However, the compressor power occupies a small portion in total regeneration duty.



250  
251 **Fig. 11.** CO<sub>2</sub> concentration of permeate gas and rich CO<sub>2</sub> loading

252 According to Eqs. 1, the required membrane area had a significant linear correlation with the  
253 average partial difference between feed and permeate gas. **Fig. 12** showed the average differential  
254 pressure and membrane area ratio under different flow ratio. The membrane area increased  
255 rapidly when the flow ratio was over 50%. When the flue gas flow ratio in membrane unit was  
256 30%, the average partial pressure difference decreased by 40%, and membrane area increased by  
257 43.67%. The optimal flow ratio was selected as 50%, and the required membrane area was about  
258 115% of 100% flow ratio condition.

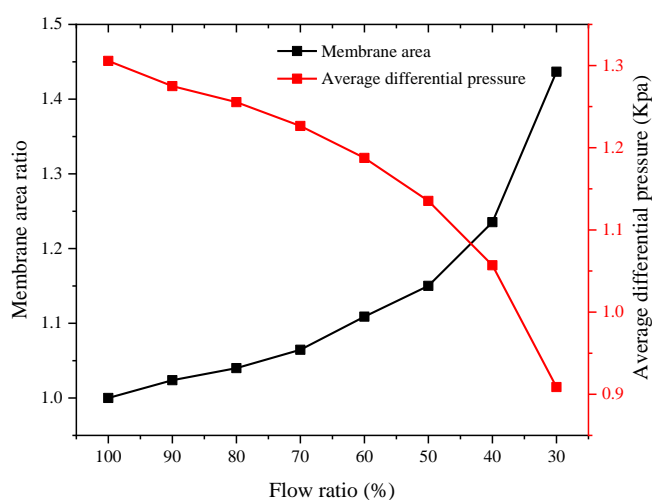


Fig. 12. Effect of flow ratio on average differential pressure and membrane area ratio.

### Pressure ratio between feed and permeate gas

To reduce the power of vacuum compressor, increasing of membrane area and decreasing of pressure difference between two sides of the membrane can be applied. While the membrane area and permeate side pressure will affect the investment cost and operating cost, these two parameters should be optimized. Table 3 showed the membrane separation, absorption and regeneration performance under different flow and pressure difference ratio. When the pressure difference ratio was 5:1. The process had lower rich CO<sub>2</sub> loading, higher compressor power and solvent regeneration duty under lower pressure difference ratio. CO<sub>2</sub> concentration of permeate gas dropped to 16.95 ~ 28.60 vol.%. The compressor power increased would rise by 10% due to greater permeate gas flow. The total regeneration duty of 5:1 pressure difference ratio increases of 2.64 ~ 3.59% compared with 10:1 pressure difference ratio. And even worse is that the membrane area was double. The optimal total regeneration duty was reduced by 20.7% when flow ratio and CO<sub>2</sub> recovery were 100% and 20% respectively.

Table 3. Membrane and absorption performance under different pressure ratio

Flow-ratio	CO <sub>2</sub> recovery	Pres-ratio	Per CO <sub>2</sub>	RLD	A <sub>mem</sub>	Q <sub>comp</sub>	Q <sub>reb</sub>
%	%	-	Vol.%	mol./mol.	m <sup>2</sup>	GJ/t CO <sub>2</sub>	GJ/t CO <sub>2</sub>
100	20	10:1	29.95	0.471	3452.57	0.1318	3.825

100	20	5:1	18.60	0.460	7293.44	0.1455	3.950
50	40	10:1	27.32	0.466	3970.73	0.1446	3.882
50	40	5:1	16.95	0.458	8255.99	0.1598	3.973

275

## 276 CONCLUSIONS

277 CO<sub>2</sub> concentration of the permeate gas, membrane area and compressor power influenced the  
 278 chemical absorption process. An integrated model with membrane mass transfer calculation  
 279 model was developed in ASPEN PLUS. The membrane calculation model could provide  
 280 permeate gas flow, composition, pressure, and required membrane area. To improve the driving  
 281 force of the gas-liquid equilibrium, the flue gas with low CO<sub>2</sub> concentration pumped into the  
 282 absorber on 19 stage. The rich CO<sub>2</sub> loading raised from 0.396 to 0.471 mol. CO<sub>2</sub> mol.<sup>-1</sup> MEA.  
 283 Under lower pressure ratio between feed with permeate side, the result showed the worse  
 284 separation performance with lower CO<sub>2</sub> concentration of permeate gas, lower rich CO<sub>2</sub> loading,  
 285 larger compressor power and larger solvent regeneration duty. The membrane area is mostly  
 286 affected by pressure ratio between feed with permeate side and flow ratio. The membrane area is  
 287 over double under lower pressure ratio and flow ratio. The optimal parameter of feed/permeate  
 288 side pressure ratio and flow ratio are 10:1 and 50% respectively. The optimal total regeneration  
 289 duty was reduced by 20.7% when flow ratio and CO<sub>2</sub> recovery were 100% and 20%, respectively.

## 290 REFERENCES

- 291 Agbonghae, E.O., Hughes, K.J., Ingham, D.B., Ma, L. and Pourkashanian, M. (2014). Optimal  
 292 process design of commercial-scale amine-based CO<sub>2</sub> capture plants. *Ind. Eng. Chem. Res.*  
 293 53:14815-14829.
- 294 Ahn, H., Luberti, M., Liu, Z.Y., and Brandani, S. (2013). Process configuration studies of the  
 295 amine capture process for coal-fired power plants. *Int. J. Greenh. Gas Control.* 16:29-40.
- 296 Akram, M., Ali, U., Best, T., Blakey, S., Finney, K.N. and Pourkashanian, M. (2016).



297 Performance evaluation of PACT pilot-plant for CO<sub>2</sub> capture from gas turbines with exhaust  
298 gas recycle. *Int. J. Greenh. Gas Control*. 47:137-150.

299 Amann, J.M.G and Bouallou, C. (2009). CO<sub>2</sub> capture from power stations running with natural  
300 gas (NGCC) and pulverized coal (PC): assessment of a new chemical solvent based on aqueous  
301 solutions of N-MethylDiEthanolAmine + TriEthylene TetrAmine. *Energy Procedia*. 1(1):909-  
302 916.

303 Artanto, Y., Jansen, J., Pearson, P., Do, T., Cottrell, A., Meuleman E. and Feron P. (2012).  
304 Performance of MEA and amine-blends in CSIRO PCC pilot plant at Loy Yang power in  
305 Australia. *Fuel*. 101: 264-275.

306 Ding, J.Y., Freeman, B. and Rochelle, G.T. (2017). Regeneration design for NGCC CO<sub>2</sub> capture  
307 with amine-only and hybrid amine/membrane. *Energy Procedia*. 114:1394-1408.

308 Frimpong, R.A., Irvin, B.D., Nikolic, H., Liu, K.L. and Figueroa J. (2019). Integrated hybrid  
309 process for solvent-based CO<sub>2</sub> capture using a pre-concentrating membrane: A pilot scale study.  
310 *Int. J. Greenh. Gas Control*. 82:204-209.

311 Freeman, B., Hao, P., Baker, R., Kniep, J., Chen, E., Ding, J., Zhang, Y. and Rochelle, G.T.  
312 (2014). Hybrid membrane-absorption CO<sub>2</sub> capture process. *Energy Procedia*. 63:605-613.

313 Le Moullec, Y. and Kanniche, M. (2011). Screening of flowsheet modifications for an efficient  
314 monoethanolamine (MEA) based post-combustion CO<sub>2</sub> capture. *Int. J. Greenh. Gas Control*.  
315 5:727-740.

316 Li, H.L., Ditaranto, M. and Berstad, D. (2011). Technologies for increasing CO<sub>2</sub> concentration in  
317 exhaust gas from natural gas-fired power production with post-combustion, amine-based CO<sub>2</sub>  
318 capture. *Energy*. 36:1124-1133.

319 Liu, B.C., Yang, X., Wang, T., Zhang, M.M. and Chiang, P.C. (2019). CO<sub>2</sub> separation by using a  
320 three-stage membrane process. *Aerosol Air Qual. Res*. 19:2917-2928.

321 Liu, F., Fang, M.X., Yi, N.T. and Wang T. (2019). Research on alkanolamine-based physical-  
322 chemical solutions as biphasic solvents for CO<sub>2</sub> capture. *Energy Fuels*. 33:11389-11398.

323 Luo, X.B., Wang, M.H. and Chen, J. (2015). Heat integration of natural gas combined cycle  
324 power plant integrated with post-combustion CO<sub>2</sub> capture and compression. *Fuel*. 151:110-117.

325 Luo, X.B., and Wang, M.H. (2016). Optimal operation of MEA-based post-combustion carbon  
326 capture for natural gas combined cycle power plants under different market conditions. *Int. J.*  
327 *Greenh. Gas Control*. 48:312-320.

328 Mangalapally, H.P., Notz, R., Asprion, N., Sieder, G., Garcia, H. and Hase, H. (2012). Pilot  
329 plant study of four new solvents for post combustion carbon dioxide capture by reactive  
330 absorption and comparison to MEA. *Int. J. Greenh. Gas Control*. 8:205-216.

331 Martín-Gamboa, M., Iribarren, D. and Dufour, J. (2018). Environmental impact efficiency of  
332 natural gas combined cycle power plants: a combined life cycle assessment and dynamic data  
333 envelopment analysis approach. *Sci. Total Environ*. 615:29-37.

334 Mores, P.L., Godoy, E., Mussati, S.F. and Scenna, N.J. (2014). A NGCC power plant with a CO<sub>2</sub>  
335 post-combustion capture option. Optimal economics for different generation/capture goals.  
336 *Chem. Eng. Res. Des*. 92: 1329-1352.

337 Mubashir, M., Fong, Y.Y., Leng, C.T. and Keong, L.K. (2018). Issues and current trends of  
338 hollow-fiber mixed-matrix membranes for CO<sub>2</sub> separation from N<sub>2</sub> and CH<sub>4</sub>. *Chem. Eng.*  
339 *Technol*. 41(2): 235-252.

340 Notz, R., Mangalapally, H.P. and Hase, H. (2012). Post combustion CO<sub>2</sub> capture by reactive  
341 absorption: pilot plant description and results of systematic studies with MEA. *Int. J. Greenh.*  
342 *Gas Control*. 6:84-112.

343 Oh, S.Y., Binns, M., Cho, H. and Kim, J.K. (2016). Energy minimization of MEA-based CO<sub>2</sub>  
344 capture process. *Appl. Energ*. 169: 353-362.

345 Rabensteiner, M., Kinger, G., Koller, M., Gronald, G. and Hochenauer, C. (2014). Pilot plant  
346 study of ethylenediamine as a solvent for post combustion carbon dioxide capture and  
347 comparison to monoethanolamine. *Int. J. Greenh. Gas Control.* 27:1-14.

348 von Harbou, I., Mangalapally, H.P. and Hasse, H. (2013). Pilot plant experiments for two new  
349 amine solvents for post-combustion carbon dioxide capture. *Int. J. Greenh. Gas Control.*  
350 18:305-314.

351 Xu, J.Y., Wang, Z., Qiao, Z.H., Wu, H.Y., Dong, S.L., Zhao S. and Wang J.X. (2019). Post-  
352 combustion CO<sub>2</sub> capture with membrane process: Practical membrane performance and  
353 appropriate pressure. *J. Membr. Sci.* 581:195–213.

354 White, L.S., Wei, X.T., Pande, S., Wu, T. and Merkel, T.C. (2015). Extended flue gas trials with  
355 a membrane-based pilot plant at a one-ton-per-day carbon capture rate. *J. Membrane Sci.*  
356 496:48-57.

357 Yang, J.Y., Yu, W., Wang, T., Liu, Z.Z. and Fang, M.X. (2020). Process simulations of the direct  
358 non-aqueous gas stripping process for CO<sub>2</sub> desorption. *Ind. Eng. Chem. Res.* 59:7121–7129.

359 Yu, C.H., Huang, C.H. and Tan, C.S. (2012). A Review of CO<sub>2</sub> Capture by absorption and  
360 adsorption. *Aerosol Air Qual. Res.* 12(5):745-769.

361 Yu, W., Wang T., Park, A.A. and Fang, M.X. (2019). Review of liquid nano-absorbents for  
362 enhanced CO<sub>2</sub> capture. *Nanoscale.* 11:17137–17156.

363 Yu, W., Wang, T., Park, A.A. and Fang, M.X. (2020). Toward sustainable energy and materials:  
364 CO<sub>2</sub> capture using microencapsulated sorbents. *Ind. Eng. Chem. Res.* 59: 9746–9759.

365